International Journal of Fracture **110:** 175–187, 2001.

Mixed-mode fracture analyses of plastically-deforming adhesive joints

Q.D. YANG[1] and M.D. THOULESS[1,2]
[1]*Department of Mechanical Engineering, University of Michigan, Ann Arbor, MI 48109-2125, USA*
[2]*Department of Materials Science & Engineering, University of Michigan, Ann Arbor, MI 48109-2125, USA*

Received 25 April 2000; accepted in revised form 30 January 2001

Abstract. A mode-dependent embedded-process-zone (EPZ) model has been developed and used to simulate the mixed-mode fracture of plastically deforming adhesive joints. Mode-I and mode-II fracture parameters obtained from previous work have been combined with a mixed-mode failure criterion to provide quantitative predictions of the deformation and fracture of mixed-mode geometries. These numerical calculations have been shown to provide excellent quantitative predictions for two geometries that undergo large-scale plastic deformation: asymmetric T-peel specimens and single lap-shear joints. Details of the deformed shapes, loads, displacements and crack propagation have all been captured reasonably well by the calculations.

Key words: Adhesion, fracture, mechanical testing, mode-mixedness, plasticity, numerical modeling.

1. Introduction

Mode-I and mode-II embedded-process-zone (EPZ) models for plastically-deforming adhesive joints have been developed by Yang et al. [1999, 2000a, 2000b]. In the approach used in these models it is assumed that the role of the adhesive layer is one merely of providing tractions between the adherends. Opening and shear traction-separation laws appropriate for a particular thickness of a commercial adhesive and a given strain rate were obtained, and it was demonstrated that excellent quantitative predictions for the fracture of adhesive joints under pure opening and pure shear could be calculated (Yang et al., 1999, 2000b). In the present paper, it is shown how the approach can be extended to mixed-mode conditions. Specifically, plastically-deforming asymmetrical T-peel and single lap-shear joints serve as two model mixed-mode geometries that are studied in detail.

Single lap-shear specimens are mixed-mode configurations frequently used for test purposes. Historically, two types of analysis have been developed in parallel for these joints: strength and fracture-mechanics approaches. The strength approach involves a stress analysis of the joint coupled with a stress- or strain-based failure criterion (Hart-Smith, 1973; Harris and Adams, 1984; Tsai et al., 1998; Adams and Wake, 1984; Bigwood and Crocombe, 1990, 1992), and dates back to the original work of Goland and Reissner (1944). However, suitable failure criteria based on a maximum stress or strain have not been well-established (Lee, 1991). The fracture-mechanics approach uses an energy-based failure criterion such as a critical energy-release rate or a critical J-integral (Anderson et al., 1988; Chai, 1988; Fernlund and Spelt, 1991; Fernlund et al., 1994; Papini et al., 1994; Tong, 1996), and relies on a knowledge of the mixed-mode failure criterion for the adhesive layer. However, this approach is subject to the limitation that the adherends can exhibit only elastic behavior before failure. When the bonding is reasonably strong or the adherends are relatively thin, the failure of a single

lap-shear joint is often accompanied by extensive plastic deformation in the adherends. As a result, the 'apparent' joint strength (failure load per unit bonded area) is strongly dependent on the adherend thickness. However, there are no analytical tools that can provide a reliable correlation between the 'apparent' and the 'intrinsic' joint strength, and the design of single lap-shear joints remains very qualitative (Hart-Smith, 1993).

It appears that the inherent difficulties associated with analyzing plastically-deforming joints can be circumvented by using the EPZ modeling approach. A mixed-mode EPZ model has been used to investigate interfacial fracture of bi-material systems (Tvergaard and Hutchinson, 1993, 1996; Wei and Hutchinson, 1997, 1998). This involves a three-parameter traction-separation law with the opening and shear stresses and displacements being interdependent in such a way that the intrinsic toughness of the interface is mode-independent. However, the experimental results of Yang et al. (1999, 2000b) showed a significant difference between the values of the toughness for the two modes; this indicates that a mode-independent model is not always appropriate for the adhesive system being studied. Therefore, an alternative implementation of a mode-dependent EPZ model is required. In this paper, such a mode-dependent EPZ model is proposed. The model is used to predict the fracture of plastically-deforming asymmetrical T-peel and single lap-shear joints (Figure 1) made of an aluminum alloy and a commercial adhesive. Mode-I and mode-II EPZ models previously developed for this adhesive are used without modification in conjunction with a simple failure criterion to account for the influence of mode-mixedness on the fracture process. The approach is validated by comparisons between the predictions of the numerical results and associated experimental results.

2. Mode-dependent EPZ model

2.1. Failure criterion

A mixed-mode EPZ model that accommodates unrelated traction-separation laws for opening and shear deformation is proposed by recognizing that the total traction-separation work absorbed during fracture, G, can be separated into the opening (mode-I) and shear (mode-II) components, G_I and G_{II}, so that,

$$G = G_I + G_{II}. \tag{1}$$

The two separate components can be calculated by integration of the mode-I and mode-II traction-separation curves (Figure 2):

$$G_I = \int_0^{\delta_n} \sigma\ (\delta_n)\ \mathrm{d}\delta_n; \qquad G_{II} = \int_0^{\delta_t} \tau\ (\delta_t)\ \mathrm{d}\delta_t, \tag{2}$$

where δ_n and δ_t denote the normal and tangential displacements. These are not independent parameters; they evolve together as a natural result of the interplay between the deformation of the adherends and the details of the two traction-separation laws. A failure criterion is required to determine the critical values of the two components of G, G_I^* and G_{II}^*, at which separation of the EPZ elements occurs. The criterion used in this study is a simple one (Wang and Suo, 1990; Hutchinson and Suo, 1992):

$$G_I^*/\,\Gamma_{I0} + G_{II}^*/\,\Gamma_{II0} = 1, \tag{3}$$

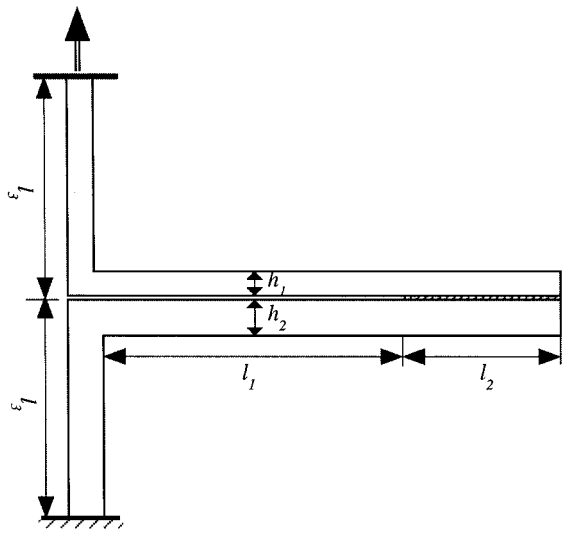

(a) Asymmetrical T-peel specimen

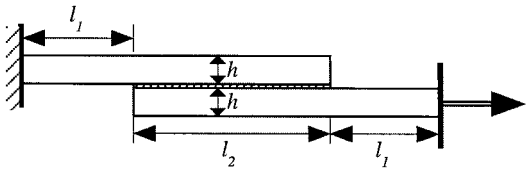

(b) Single lap-shear specimen

Figure 1. Geometries of the (a) asymmetrical T-peel specimen and (b) the single lap-shear specimen.

where Γ_{I0} and Γ_{II0} are the total areas under the opening and shear traction-separation laws.

The mode-mixedness calculation evolves naturally out of the numerical calculations, and is dependent on the fracture criterion and traction-separation laws. As loading progresses, the opening and shear displacements of the EPZ elements are determined numerically, and G_I and G_{II} are then calculated from Equation (2). When the failure criterion of Equation (3) is met, the elements fail and the crack advances. While the mode-mixedness does not need to be determined specifically in this scheme, it is often convenient to be able to define it for purposes of comparison. While it should be appreciated that definitions of mode-mixedness and the resulting values may be sensitive to the details of the fracture parameters, a phase angle can be defined as

$$\phi = tan^{-1}\left[\left(\frac{G^*_{II}}{G^*_I}\right)^{1/2}\right]. \tag{4}$$

Another quantity, G^*_I/Γ_{I0}, appeared to be more useful in providing a measure of the sensitivity of failure to the mode-II component of the traction-separation law. A value of G^*_I/Γ_{I0} close to one indicates that predictions for crack propagation are not very sensitive to the choice of mode-II fracture parameters. A mode-independent failure criterion could be used satisfactorily in such a case, or the problem could even be tackled as a pure mode-I calculation.

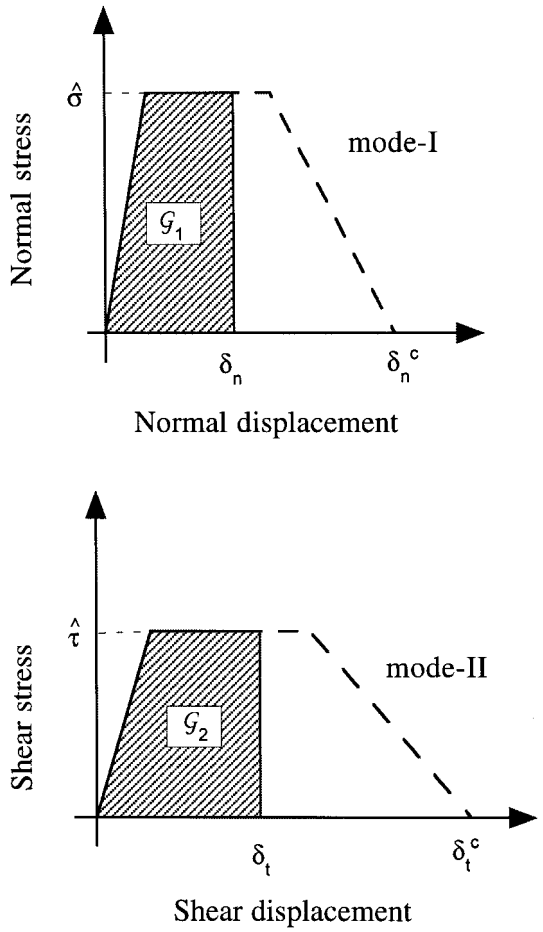

Figure 2. Schematic illustration of the mixed-mode EPZ model used in this study. G_I and G_{II} are the mode-I and mode-II traction separation energies, at normal and shear displacements of δ_n and δ_t. δ_n^c and δ_t^c are the critical normal and tangential displacements for pure mode-I and mode-II fracture.

2.2. Fracture parameters

The initial experiments indicated that mixed-mode fracture always occurred by interfacial crack propagation ('adhesive' failure). This was identical to the results of the shear tests described in Yang et al. (2000b). In contrast, the mode-I fracture parameters published in Yang et al. (1999) were obtained for crack propagation within the adhesive layer ('cohesive' failure). Therefore, it was necessary to re-determine the mode-I parameters for interfacial fracture. The technique described in Yang et al. (1999) was used – adhesively-bonded, symmetrical, double-cantilever beams (DCB) were fractured by means of a wedge forced between the adherends. However, in the present tests, an initial crack along one of the adhesive/aluminum interfaces was introduced by inserting a strip of Teflon® tape into the interface before the sample was cured. Introducing a slight asymmetry in this fashion appeared sufficient to keep the crack along one of the interfaces for the entire test. The adherends (5754 Al alloy), adhesive (XD4600 from Ciba Specialty Products) and bond-line thickness (0.25 mm) were identical to those used in all the other tests. The width of all the samples was 20 mm, and three different thickness of aluminum coupons were used (1.0 mm, 2.0 mm and 3.0 mm). A tensile test

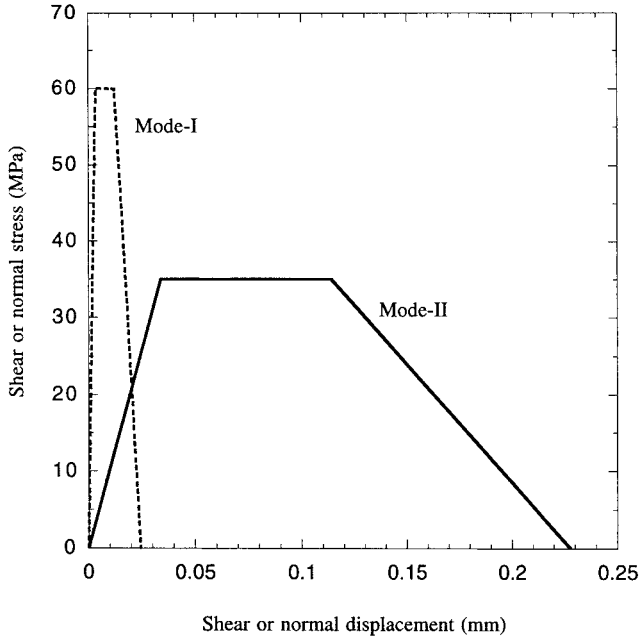

Figure 3. Details of the opening (mode-I) and shear (mode-II) traction-separation laws developed for interfacial crack growth between a 0.25 mm thick layer of an XD4600 adhesive and a 5754 aluminum alloy.

machine with a cross-head velocity of 20 mm min^{-1} was used to force the samples over a wedge with a wedge-tip diameter of 8.5 mm. After the tests were completed, the radii of the deformed portions of the beams were measured and compared to predictions of a mode-I EPZ calculation to determine which values of the fracture parameters gave the best fit to the data. It was found that for 'adhesive' failure (with the crack running at an interface), a peak normal stress of $\hat{\sigma} = 60 \pm 10$ MPa and a mode-I toughness of $\Gamma_{I0} = 1.0 \pm 0.15$ kJ m^{-2} provided the best fit. This is in contrast to $\hat{\sigma} = 100$ MPa and $\Gamma_{I0} = 1.4 \pm 0.15$ kJ m^{-2} for 'cohesive' failure (with the crack running through the adhesive layer) in the same specimens (Yang et al., 1999). Details of the interfacial shear traction-separation law previously determined in Yang et al. (2000b) (a peak shear stress of $\hat{\tau} = 35$ MPa and a mode-II toughness of $\Gamma_{II0} = 5.4$ kJ m^{-2}) and the interfacial opening traction-separation law determined here are illustrated in Figure 3. These models allow quantitative predictions of pure mode-I and pure mode-II interfacial crack growth; in this paper they are used without any further modification to predict mixed-mode fracture of asymmetrical T-peel joints and single lap-shear joints.

3. Experimental and numerical studies of mixed-mode fracture

The results of the numerical calculations that follow were obtained by incorporating the traction-separation laws of Figure 3 and the mixed-mode criterion of Eqn.3 into elastic-plastic finite-element calculations. The ABAQUS code (version 5.8) with large-strain and large-rotation conditions was used. Four-point bi-linear, reduced-integration, 2-D elements were used to model the adherends[1]. The mechanical behavior of the adherends was simulated

[1]Plane-strain elements were used for the asymmetric T-peel specimens because their deformation is dominated by bending. Plane-stress elements were used for the shear-lap geometry because the deformations in the free arms are dominated by axial tension.

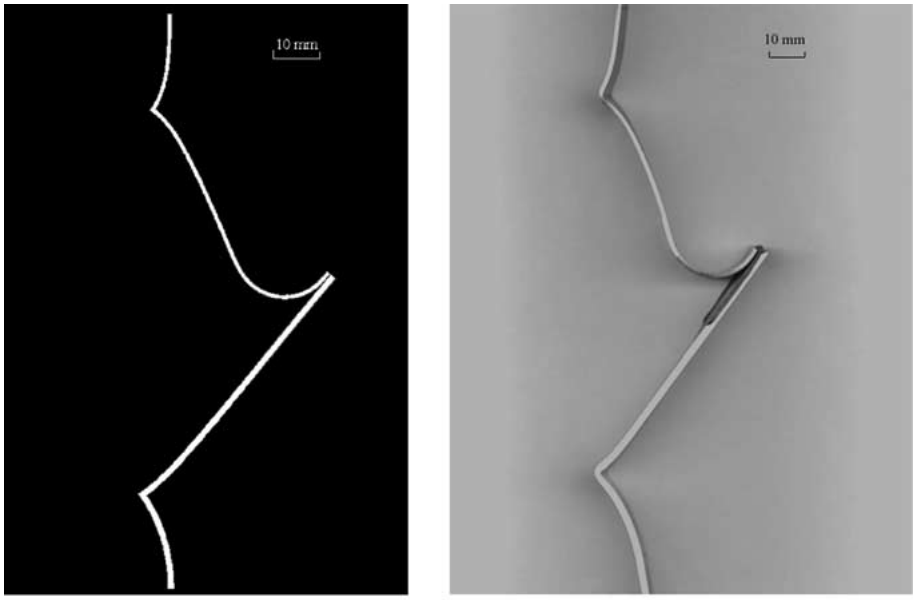

Figure 4. (a) The predictions from the numerical model for the deformation of an asymmetrical T-peel specimen (1.3/2.0 mm). (b) Micrograph of a fractured asymmetrical T-peel specimen (1.3/2.0 mm).

using the elastic-plastic constitutive properties previously determined by a uniaxial tensile test (see Yang et al., 2000b), with additional assumptions of the von Mises yield criterion and isotropic strain-hardening. After the calculations were completed for each geometry, the load-displacement curves and deformed shapes of the joints predicted by the numerical calculations were compared to experimental observations.

3.1. Asymmetrical T-peel test

The geometry for the asymmetrical T-peel test is shown in Figure 1a. The materials used, sample preparation, and experimental procedures are almost identical to that described in Yang et al. (1999) for symmetrical T-peel joints, except that, here, different thicknesses of aluminum coupons were bonded together. For all the samples used in this study, the initial crack length (l_1) was 60 mm, the length of bond-line (l_2) was 30 mm, and the length of the bent portion of the arms (l_3) was 30 mm. The adhesive thickness was maintained at 0.25 mm by the use of uniform-sized silica spheres as spacers. Three adherend thickness combinations, $h_1/h_2 = 1.0/2.0$ mm, 1.3/2.0 mm, and 1.6/2.0 mm, were studied.

Figure 4 compares the numerically-predicted and experimentally-observed deformation of a 1.3/2.0 mm sample. Clearly, the numerical calculations quantitatively capture all the features of the deformation, including the large strains and rotations, the extent of fracture, and the asymmetry of bending. A comparison between the observed load-displacement plots and those predicted numerically are shown in Figure 5. The shaded areas in these plots indicate the range of experimental data from five specimens for each thickness combination, and the dashed lines are the associated numerical predictions. It can be seen that the numerical calculations do an excellent job of reproducing the entire deformation history of the asymmetrical T-peel joints. Both the shapes of the curves and the magnitudes of the peel forces are sensitive to thickness

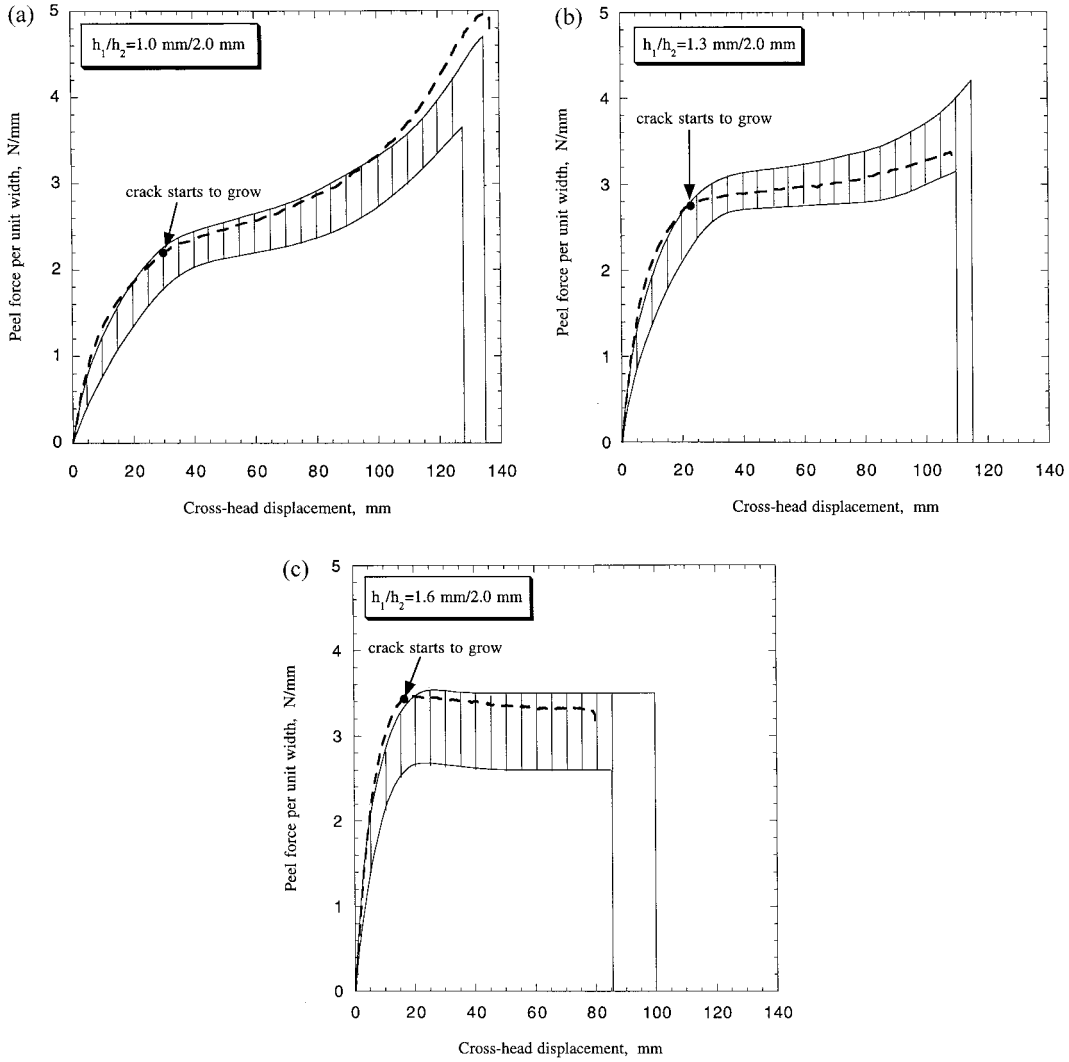

Figure 5. Comparisons of numerically-predicted and experimentally-measured peel force (per unit width) as a function of cross-head displacement. The shaded areas indicate the range of results for a series of nominally identical experiments. The dashed lines show the numerical predictions. (a) $h_1/h_2 = 1.0/2.0$ mm; (b) $h_1/h_2 = 1.3/2.0$ mm; (c) $h_1/h_2 = 1.6/2.0$ mm.

of the adherends, yet the numerical calculations not only reproduce the magnitude of the peel force, but also capture some of the nuances of the shape of the load-displacement curves.

The phase angle predicted by Equation (4) for the 1.3/2.0 mm asymmetrical T-peel specimen was approximately 28°, and was found to be relatively independent of crack extension. The ratio of G_I^*/Γ_{I0} was equal to 0.95, which makes it clear that fracture of this geometry is dominated by the mode-I parameters. Indeed, a series of additional numerical experiments showed that the peel forces for all the asymmetrical T-peel joints were very sensitive to the mode-I parameters, but were fairly insensitive to the mode-II parameters. This geometry, therefore, has the characteristic of being essentially mode-I dominated. A contrast is provided by the next example studied, the single lap-shear geometry, for which the use of reliable mode-II parameters proved to be essential in obtaining accurate predictions of fracture.

(a) Numerical predictions

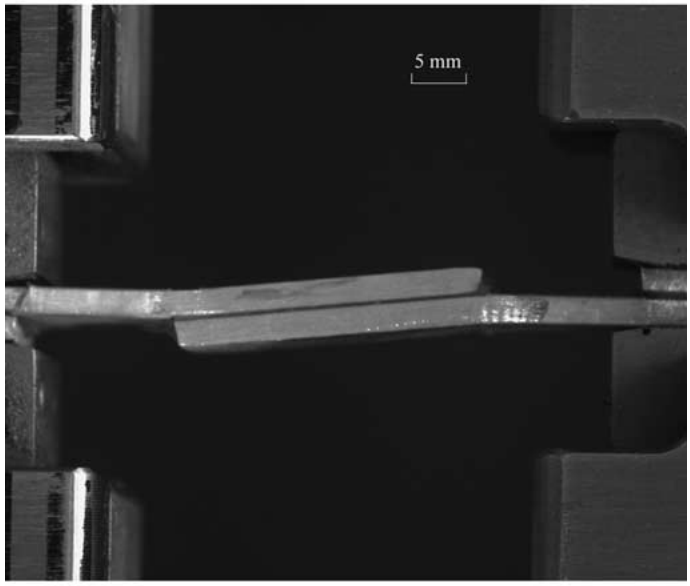

(b) Experimental observations

Figure 6. Global deformation of a 2.3 mm-thick single lap-shear specimen at the point of crack initiation: (a) numerical predictions, (b) experimental observations.

3.2. SINGLE LAP-SHEAR TEST

The single lap-shear test configuration is illustrated in Figure 1(b). For all the specimens used in this study, the length of the bond-line (l_2) was 25.4 mm and the length of the free arm (l_1) was 12.7 mm. The adherend thickness (h) ranged from 1.6 to 3.0 mm, and the adhesive thickness was 0.25 mm. To facilitate *in-situ* optical observations during the fracture process, straight lines were cut across the bond-lines using a sharp razor. During the test, one end of the sample was held fixed by a tensile test machine and the other end was held by a grip that moved at a constant velocity of 1 mm min^{-1}. A high-resolution CCD camera was used to measure the actual displacement between the two ends of the sample. In addition, the CCD camera was used to observe the crack initiation and propagation, and to observe the deformation of the adhesive layer near the crack-tip.

Comparisons between the numerically-predicted global deformation of a 2.3 mm sample and the experimentally-observed deformation are given in Figures 6 and 7. Figure 6 shows the specimen at the point at which the crack is initiated, and Figure 7 shows the specimens

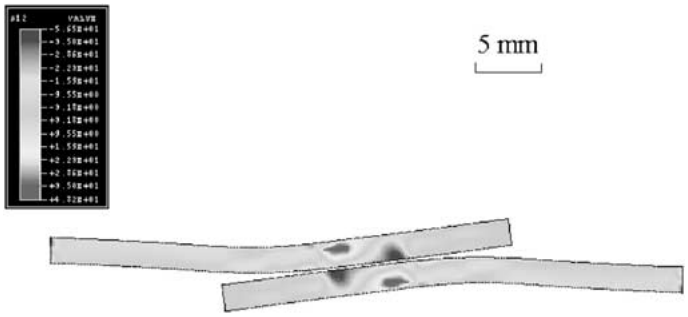

(a) Numerical predictions

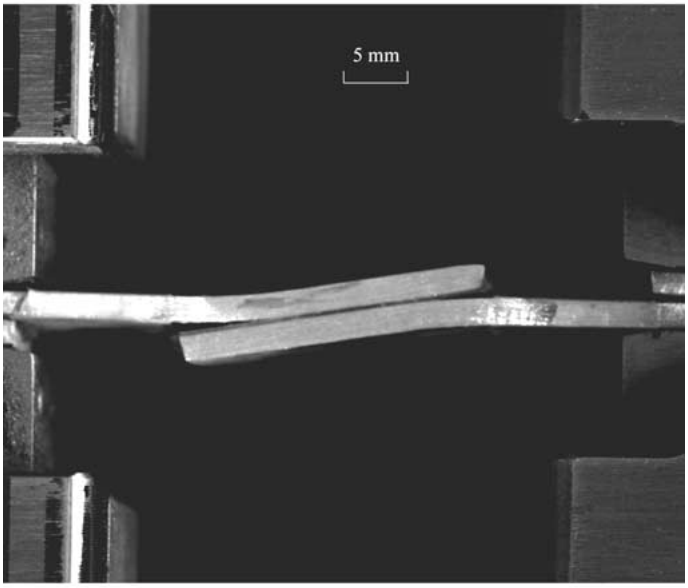

(b) Experimental observations

Figure 7. Global deformation of a 2.3 mm thick single lap-shear specimen just before the onset of unstable crack growth (a) numerical predictions, (b) experimental observations.

just before the onset of final failure. It should be noted that the grips had some freedom to rotate. Therefore, although the specimens were well-aligned at the beginning of each test, the bending moment induced by the lap-shear geometry caused a re-alignment that can be seen from Figures 6 and 7. However, this re-alignment was not modeled in the numerical calculations in which it was assumed that the grips were perfectly rigid. The extensive deformation that occurs in the adhesive layer near the crack tip can be observed in Figure 8. The shear strain was about 18% at crack initiation (Figure 8(a)), and increased as the crack propagated (28% in Figure 8(b)) to a maximum of about 40% immediately before the onset of unstable crack growth (Figure 8(c))[2]. The large shear that can be observed in the single lap-shear joints is in distinct contrast to the asymmetric T-peel joints, where the deformations were too small to be measured reliably. This emphasizes why the mode-II fracture parameters needed

[2]While the normal strain appeared to be about 3–6% throughout the experiments, the resolution of the CCD camera was not able to provide a more accurate measurement.

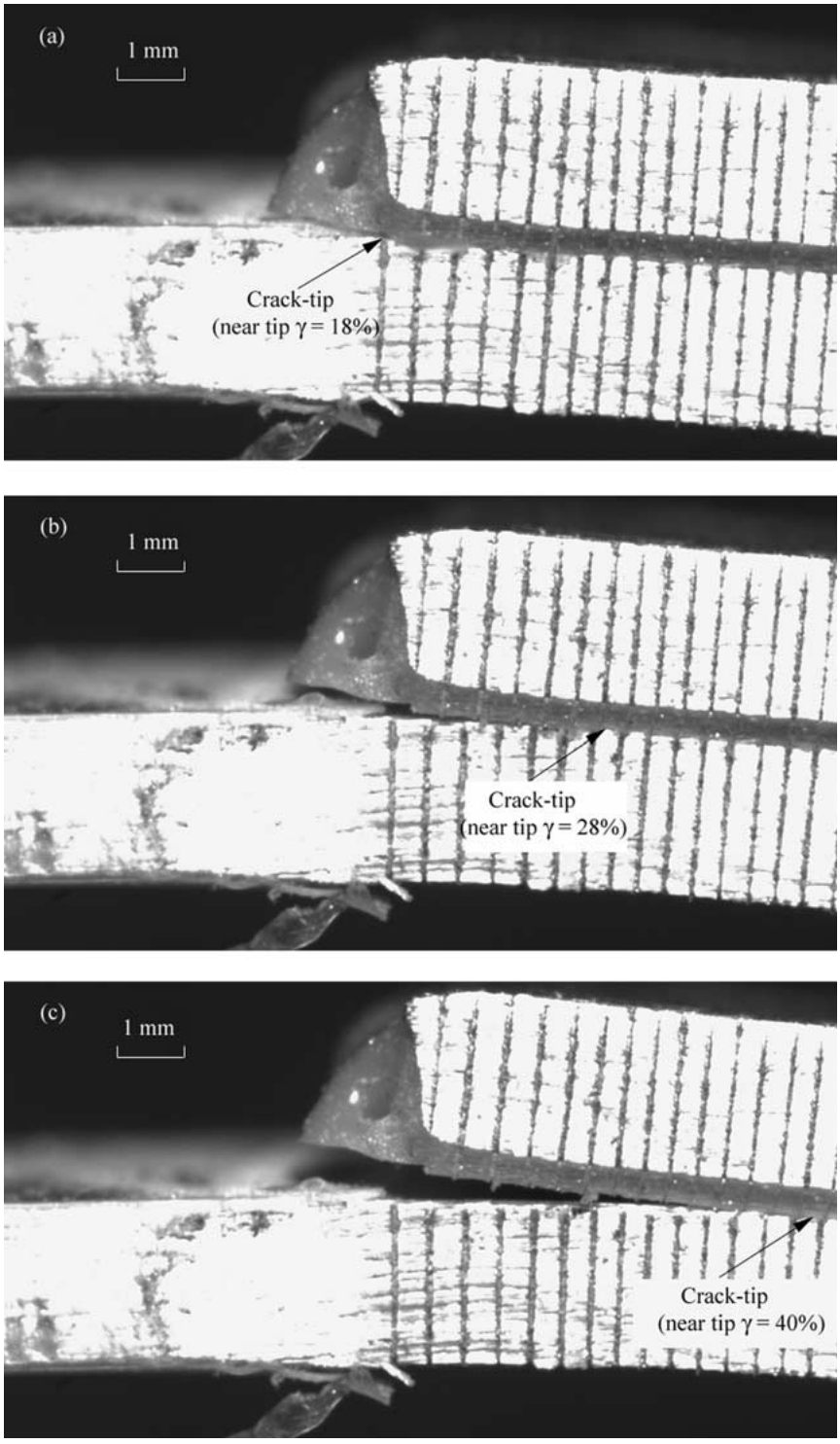

Figure 8. Deformation in the adhesive of a 2.3 mm-thick single lap-shear specimen (a) at the point of crack initiation, (b) at an intermediate stage of crack propagation and (c) immediately before the onset of unstable crack growth.

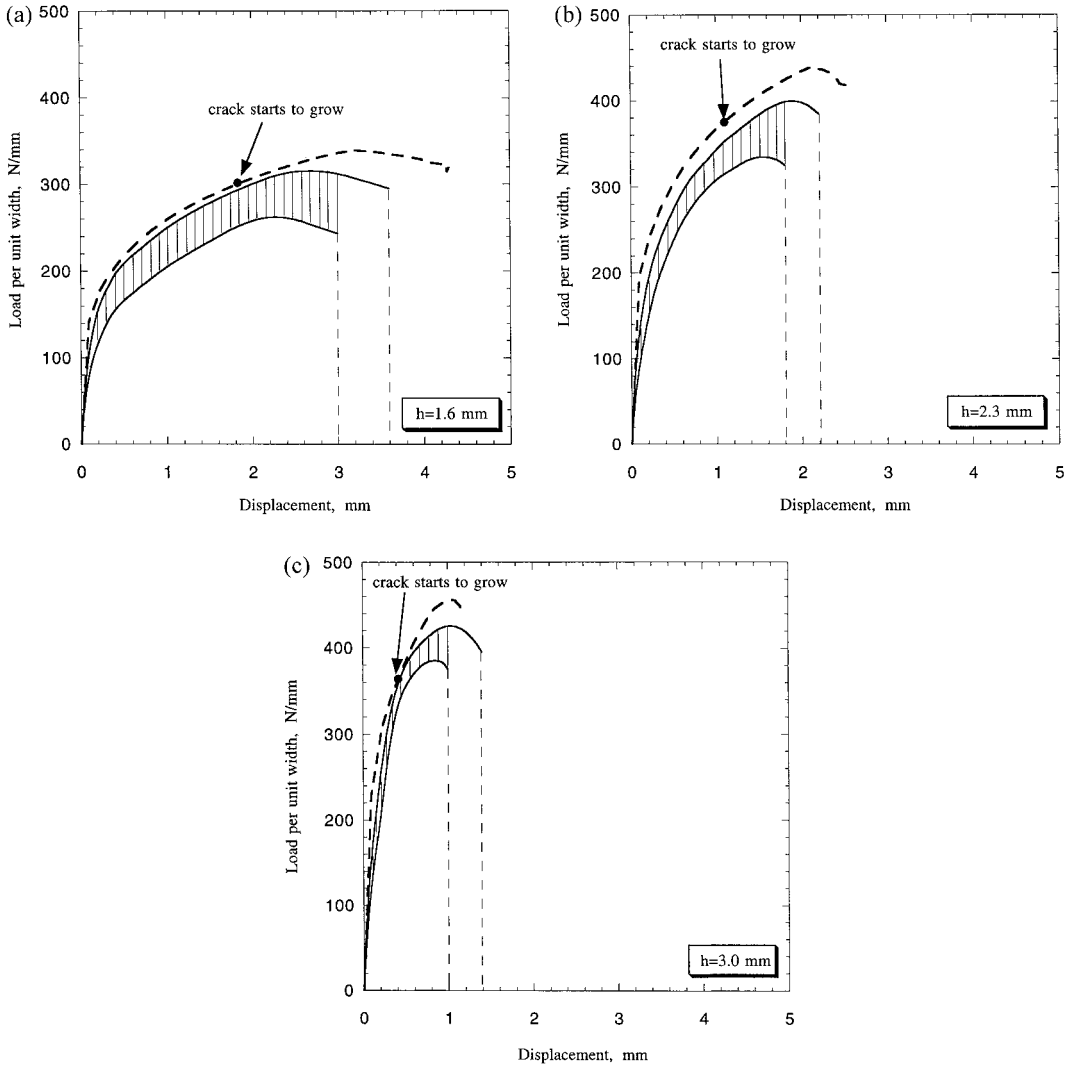

Figure 9. Comparisons of numerically predicted and experimentally measured shear-lap force (per unit width) as a function of cross-head displacement The shaded areas show the range of results of a series of experiments. The dashed lines shows the numerical prediction. (a) $h = 1.6$ mm, (b) $h = 2.3$ mm, (c) $h = 3.0$ mm.

to be accurately included in the numerical modeling of the lap-shear joints, but were not so significant for the T-peel joints.

Figure 9 compares the numerically-predicted load-displacement curves of three different single lap-shear joints with the associated experimental results. In this figure, the shaded areas represent the range of experimental data for several specimens of each thickness. The dashed lines are the numerical results. Again, the numerical simulations did a very satisfactory job of predicting the load-deformation behavior of the joints. They captured the dependence of the fracture loads and the final strain on the adherend thickness, and they demonstrated the progressive nature of the crack propagation between the initiation and the onset of unstable crack growth. In particular, it should be noted that the maximum loads in Figure 9 correspond neither to crack initiation nor to the onset of instability. An example of the mode-mixedness associated with the numerical calculations is shown in Figure 10. Both the phase angle pre-

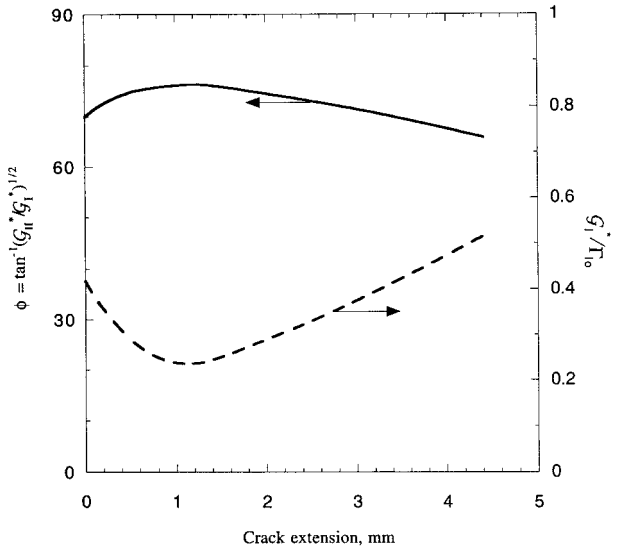

Figure 10. Numerically-predicted phase angle and G_I^*/Γ_{I0} plotted as functions of crack extension for the 2.3 mm thick single lap-shear joint.

dicted by Equation (4), and the ratio G_I^*/Γ_{I0} show how significant the shear component is. Again, this emphasizes why inclusion of the mode-II fracture parameters was so much more important for the numerical modeling of the slap-shear geometry than for the T-peel geometry.

4. Conclusions

A mode-dependent EPZ model has been used to simulate the mixed-mode fracture of plastically-deforming adhesive joints. Mode-I and mode-II fracture parameters obtained from previous work have been combined with a mixed-mode failure criterion to provide quantitative predictions of the deformation and fracture of two mixed-mode geometries: asymmetrical T-peel joints and single lap-shear joints. It has been shown that the numerical calculations using this model provide excellent quantitative predictions for the fracture of these joints failing with very large plastic deformation. In particular, it is the first time that the deformation and failure of plastically-deforming lap-shear joints have been quantitatively predicted. It appears that the approach described in this paper provides a powerful and general tool that can be used to predict quantitatively the behavior of adhesive joints.

Acknowledgements

This work was supported by NSF Grant CMS-9624452 and Ford Motor Company. The support and help of Dr Susan Ward and Dr John Hill are particularly appreciated.

References

Adams, R.D. and Wake, W.C. (1984). *Structural Adhesive Joints in Engineering*, Elsevier Applied Science Publisher, London.

Anderson, G.P., Brinton, S.H., Ninow, K.J. and DeVries, K.L. (1988). A fracture mechanics approach to predicting bond strength. In: *Advances in Adhesively-Bonded Joints*, ASME, New York, 93–101.

Bigwood, D.A. and Crocombe, A.D. (1990). Nonlinear adhesive bonded joint design analysis. *International Journal of Adhesion and Adhesives* **10**, 31–41.

Bigwood, D.A. and Crocombe, A.D. (1992). Development of a full elasto-plastic adhesive joint design analysis. *Journal of Strain Analysis* **27**, 211–218.

Chai, H. (1988). Shear fracture. *International Journal of Fracture* **37**, 137–159.

Fernlund, G., Papini, M., McCammond, D. and Spelt, J.K. (1994). Fracture load predictions for adhesive joints. *Composite Science and Technology* **51**, 587–600.

Goland, M. and Reissner, E. (1944). The stresses in cemented joints. *Journal of Applied Mechanics* **66**, A17–A27.

Harris, J.A. and Adams, R.D. (1984). Strength prediction of bonded single lap joints by nonlinear finite element methods. *International Journal of Adhesion and Adhesives* **4**, 65–78.

Hart-Smith, L.J. (1973). *Adhesive-Bonded Single Lap Joints*, Langley Research Center, NASA CR-112236, Hampton, Virginia.

Hart-Smith, L.J. (1981). *Developments in Adhesives II.* (Edited by Kinloch, A.J.), Applied Science Publisher, New York.

Hart-Smith, L.J. (1993). The bonded lap-shear test coupon – useful for quality assurance but dangerously misleading for design data. *The 38th International SAMPE Symposium*, 239–246.

Hutchinson, J.W. and Suo, Z. (1992). Mixed mode cracking in layered materials. *Advances in Applied Mechanics* **29**, 63–191.

Lee, L.H. (1991). *Adhesive Bonding*, Plenum Press, New York.

Papini, M., Fernlund, G. and Spelt, J.K. (1994). The effect of geometry on the fracture of adhesive joints. *International Journal of Adhesion and Adhesives* **14**, 5–13.

Tong, L. (1996). Bond strength for adhesive bonded single lap joints. *Acta Mechanica* **117**, 103–113.

Tsai, M.Y., Oplinger, D.W. and Morton, J. (1998). Improved theoretical solutions for adhesive lap joints. *International Journal of Solids and Structures* **35**, 1163–1185.

Tvergaard, V. and Hutchinson, J.W. (1993). The influence of plasticity on the mixed-mode interface toughness. *Journal of the Mechanics and Physics of Solids* **41**, 1119–1135.

Tvergaard, V. and Hutchinson, J.W. (1996). On the toughness of ductile adhesive joints. *Journal of the Mechanics and Physics of Solids* **44**, 789–800.

Wang, J.S. and Suo Z. (1990). Experimental determination of interfacial toughness using Brazil-nut-sandwich. *Acta Metallurgica* **38**, 1279–1290.

Wei, Y. and Hutchinson, J.W. (1997). Nonlinear delamination mechanics for thin films. *Journal of the Mechanics and Physics of Solids* **45**, 1137–1159.

Wei, Y. and Hutchinson, J.W. (1998). Interface strength, work of adhesion and plasticity in the peel test. *International Journal of Fracture* **93**, 315–333.

Yang, Q.D., Thouless, M.D. and Ward, S.W. (1999). Numerical simulations of sdhesively-bonded beams failing with extensive plastic deformation. *Journal of the Mechanics and Physics of Solids* **47**, 1337–1353.

Yang, Q.D., Thouless, M.D. and Ward, S.W. (2000a). Analysis of the symmetrical 90°-peel test with extensive plastic deformation. *Journal of Adhesion* **72**, 115–132.

Yang, Q.D., Thouless, M.D. and Ward, S.W. (2000b). Elastic-plastic mode-II fracture of adhesive joints. *International Journal of Solids and Structures* (in press).